EURASIAN PHYSICAL TECHNICAL JOURNAL

2025, Volume 22, No.4 (54)

https://doi.org/10.31489/2025N4/101-116

Received: 13/05/2025 Revised: 26/10/2025 Accepted: 22/12/2025 Published online: 29/12/2025

Original Research Article

UDC 53.01

COMPUTATIONAL ANALYSIS OF INFORMATION-THEORETIC MEASURES AND OSCILLATOR STRENGTHS IN QUANTUM SYSTEMS VIA THE NIKIFOROV–UVAROV METHOD

Inyang E.P.[1]*, Okoi P.O.[2], Nwachukwu I.M.[1]

[1] Department of Physics, Faculty of Science, National Open University of Nigeria, Jabi-Abuja, Nigeria
[2] Department of Physics, Faculty of Physical Science, University of Calabar, Calabar, Nigeria
*Corresponding Author: etidophysics@gmail.com;einyang@noun.edu.ng

Abstract. *This study investigates Fisher and Shannon entropies in one- and three-dimensional systems under the Radial Scalar Power Potential. Using the Nikiforov–Uvarov method combined with the Greene–Aldrich approximation, we derived energy eigenvalues and normalized wavefunctions. The results demonstrate that Shannon and Fisher entropies satisfy fundamental quantum information inequalities, including the Białynicki–Birula–Mycielski and Stam–Cramér–Rao bounds, across different spatial dimensions. Rényi entropy was also analyzed in both position and momentum spaces, revealing its dependence on the screening parameter and highlighting the complementarity in measurement precision between conjugate domains. In particular cases, the Radial Scalar Power Potential reduces to the Kratzer potential, allowing the computation of energy spectra for methylidyne (CH) and nitrogen (N_2) molecules. Energy increases with angular momentum, affecting molecular stability and spectroscopic transitions, while calculated oscillator strengths are in agreement with previous results, thereby validating the Radial Scalar Power Potential model for applications in both quantum information theory and molecular spectroscopy.*

Keywords: Schrödinger equation, Oscillator strength, Nikiforov-Uvarov method; Diatomic molecules; Entropic uncertainty

1. Introduction

Quantum information theory studies the transfer and manipulation of information within quantum systems by combining principles from quantum mechanics, computer science, and information theory. It focuses on understanding and controlling how information is stored in quantum states. Among the various metrics used in this field, Shannon entropy and Fisher information have been widely applied [1, 2], as they provide a rigorous way to quantify uncertainty in atoms and molecules. Over the years, information-theoretic measures in quantum systems have attracted significant attention [3], largely due to their applications in probability density functions and computational analyses, offering deeper insights into the behavior of quantum mechanical systems. These measures have been applied across diverse areas, including physical and chemical sciences [4]. The entropic uncertainty relation serves as an alternative formulation to the Heisenberg uncertainty principle [5]. In both position and momentum spaces, information-theoretic tools have been extensively employed to study the distribution of quantum states under various potential models [1-5]. In

.

quantum mechanics, the Heisenberg uncertainty principle (HUR) [6] was later reformulated in terms of entropies by Białynicki-Birula and Mycielski (BBM) [7], extending its application to both position and momentum spaces. However, Hirschman [8] was the first to introduce an entropic approach to the position-momentum uncertainty relation, and Beckner [9] provided a formulation equivalent to BBM, highlighting the crucial role of entropy in capturing the intrinsic uncertainty of quantum systems. This entropic relation is expressed as:

$$S(\rho_{nl}) + S(\gamma_{nl}) \geq D(1 + ln\,\pi) \quad (1)$$

The number of spatial dimensions is denoted by D. This relationship has been shown to surpass the Heisenberg Uncertainty Relation (HUR) in sophistication, as it can accommodate greater complexity. The Shannon entropy, a key metric in this framework, is defined as:

$$S(\rho_{nl}) = -\int_{R^D} \rho_{nl}(r_q)\, ln\, \rho_{nl}\,(r_q) dr_q \quad (2)$$

,

and

$$S(\gamma_{nl}) = -\int_{R^D} \gamma_{nl}(p)\, ln\, \gamma_{nl}\,(p) dp \ , \quad (3)$$

where $S(\rho_{nl})$ is the position space Shannon entropy, $S(\gamma_{nl})$ is the momentum space Shannon entropy, R^Drepresent integrating over real space and D is the dimensions which could be 1,2 or 3.

The probability densities (PD) in position and momentum spaces are provided in Equations (4) and (5), respectively.

$$\rho_{nl}(r_q) = \left|\psi(r_q)\right|^2 \quad (4)$$

and

$$\gamma_{nl}(p) = |\psi(p)|^2 \quad (5)$$

$\boldsymbol{\psi(p)}$ represents the momentum-space wave function, obtained by applying the Fourier transform (FT) to $\boldsymbol{\psi(r_q)}$**.** This concept is related to Shannon entropy and reflects the degree to which a system is localized or spread out in space [10]. In contrast, Fisher information (FI), a purely local measure, primarily investigates local variations in the probability density (PD) and is expressed as follows [11]:

$$I(\rho) = \int_{R^D} \frac{|\nabla \rho_{nl}(r_q)|^2}{\rho_{nl}(r_q)} dr_q \quad (6)$$

$$I(\gamma) = \int_{R^D} \frac{|\nabla \rho_{nl}(p)|^2}{\rho_{nl}(p)} dp \quad . \quad (7)$$

Fisher information inequality becomes [11]

$$I(\rho)I(\gamma) \geq 9\left[2 - \frac{2l+1}{l(l+1)}|m|\right]^2 \geq 36\,. \quad (8)$$

The Rényi entropy [12] in coordinate spaces can be expressed as

$$R_q(\rho_r) = \frac{1}{1-q}\mathrm{In}\left(\int_{R^D}\left|\rho(r_q)\right|^q dr_q\right) \quad (9)$$

$$R_q(\phi_p) = \frac{1}{1-q}\mathrm{In}\left(\int_{R^D}|\phi(p)|^q dp\right) \quad (10)$$

The concept of Rényi entropy introduces an index parameter q, which characterizes the sensitivity of a system to deviations from equilibrium. When q=1, Rényi entropy reduces to Shannon entropy, representing the equilibrium distribution and reflecting the balance of uncertainty in the system. For q>1, Rényi entropy decreases, indicating increased knowledge about the system, whereas for q<1, the entropy rises, reflecting reduced information. The parameter q is always non-negative and lies within the range $0 \prec q \prec \infty$ [13]. Previous studies have applied information-theoretic measures to molecular systems. Amadi et al. [14] investigated

Shannon entropy and Fisher information in three-dimensional molecular systems under the Deng-Fan and Eckart potentials for diatomic molecules, finding that Shannon entropy exhibited localization, while Fisher information indicated delocalization in both position and momentum spaces. Both measures satisfied the BBM and Stam–Cramér–Rao (SCR) inequalities. Similarly, Onyeaju et al. [15] analyzed Shannon and Rényi entropies in molecular potentials, validating the Heisenberg Uncertainty Principle (HUP) through expectation values in both position and momentum spaces. Laguna et al. [16] further explored information-theoretic measures using Gaussian-type functions.

Oscillator strength, which quantifies the probability of an electron transition between energy levels in atoms or molecules, is critical for understanding spectral line intensities and matter–radiation interactions [17,18]. For instance, Hibbert [19] described oscillator strength as a measure of electric dipole emission during electron transitions, using the dipole approximation and selection rules. This measure has been widely applied in stellar spectroscopy, where atomic transitions involve energy absorption or emission. Studies on oscillator strengths in different potential models have produced diverse trends. Ikot et al. [20] found that oscillator strength decreased with increasing potential parameters in the enhanced molecular Manning–Rosen potential, while Varshni [21] observed a similar decrease under the Hulthén potential. In contrast, Hassanabadi et al. [22] reported an increase in oscillator strength for the generalized Pöschl–Teller potential as potential parameters were raised. Numerous other studies have examined potential models in quantum systems [23–25].

However, to the best of our knowledge, no previous work has applied the Radial Scalar Power Potential (RSPP) to investigate Fisher information, Shannon and Rényi entropies, or oscillator strengths in coordinate spaces. The RSPP provides a valuable framework for analyzing quantum state behavior, calculating information-theoretic measures, and determining transition probabilities, which are essential for advancing quantum information theory and understanding oscillator strengths. Accordingly, this study investigates Shannon, Fisher, and Rényi entropies, oscillator strength, and the energy spectra of methylidyne (CH) and nitrogen (N_2) diatomic molecules within the context of the RSPP.

2. The solutions for the eigenvalues and wavefunctions.

In this study, we employ the Nikiforov-Uvarov (NU) method [26], a systematic technique for solving second-order differential equations of the hypergeometric form. For a comprehensive derivation and detailed methodology, refer to Appendix A. When examining a quantum system governed by a defined potential, the Schrödinger equation (SE) is represented as [27]:

$$\frac{d^2R_{nl}(r_q)}{dr_q{}^2}+\frac{2\mu}{\hbar^2}\left(E_{nl}-V(r_q)-\frac{l(l+1)\hbar^2}{2\mu r_q{}^2}\right)R_{nl}(r_q)=0 \tag{11}$$

where l is the angular momentum quantum number, μ is the reduced mass , $r_q$is the particle distance, and $\hbar$ is the Planck constant.

The RSPP is of the form [28]

$$V(r_q)=a_0r_q+b_0r_q{}^2+d_0-\frac{g_0}{r_q}+\frac{k_0}{r_q{}^2} \tag{12}$$

where a_0, b_0, d_0, g_0,and k_0 are potential strength.

The RSPP has valuable practical and experimental implications in quantum mechanics, atomic physics, and molecular systems. It offers a more precise model for studying particle interactions in central force fields, especially in cases where traditional potentials like the Coulomb or harmonic oscillator fall short in capturing interaction details. Experimentally, this potential helps predict energy spectra and analyze the behavior of diatomic molecules, quarkonium systems, and nanoscale particles. Its flexibility makes it ideal for fitting experimental data more accurately, leading to a deeper understanding of complex physical phenomena like the information theory.

Inserting Eq. (12) into (11) gives

$$\frac{d^2R_{nl}}{dr_q{}^2}+\frac{2\mu}{\hbar^2}\left(E_{nl}-a_0r_q-b_0r_q{}^2-d_0+\frac{g_0}{r_q}-\frac{k_0}{r_q{}^2}-\frac{l(l+1)\hbar^2}{2\mu r_q{}^2}\right)R_{nl}(r_q)=0\,, \tag{13}$$

.

Equation (13) cannot be solved exactly with the inserted potential model. The Greene-Aldrich approximation scheme $r_q^{-2} \approx \alpha^2(1-e^{-\alpha r_q})^{-2}; r_q^{-1} \approx \alpha(1-e^{-\alpha r_q})^{-1}$ is employed to address the centrifugal barrier. This approximation provides a reliable estimate for the centrifugal term and is applicable within the range specified by $\alpha << 1$, [29]. The Greene-Aldrich approximation is selected for its simplicity and effectiveness in solving Schrödinger equation with specific potential forms. However, its limitations arise in higher-dimensional scenarios due to reduced accuracy in capturing the intricate coupling of angular momentum and potential terms, which may lead to deviations in energy eigenvalues and wavefunction behavior. By applying a variable transformation from $r_q \to x_d$, our new coordinate is expressed in terms of the parameter $x_d = e^{-\alpha r_q}$, which enables the simplification of Eq. (13), ultimately leading to Eq. (14).

$$\frac{d^2\psi(x_d)}{dx_d{}^2} + \frac{1-x_d}{x_d(1-x_d)}\frac{d\psi(x_d)}{dx_d} + \frac{1}{[x_d(1-x_d)]^2}\begin{bmatrix} -A(1-x_d)^4 - B(1-x_d)^3 \\ -\varepsilon(1-x_d)^2 + C(1-x_d) - D - \gamma \end{bmatrix}\psi(x_d) = 0, \tag{14}$$

where

$$-\varepsilon = \frac{2\mu E_{nl}}{\alpha^2\hbar^2} - \frac{2\mu d_0}{\alpha^2\hbar^2}, \quad A = \frac{2\mu a_0}{\alpha^4\hbar^2}, \quad B = \frac{2\mu b_0}{\alpha^3\hbar^2}, \quad C = \frac{2\mu g_0}{\alpha\hbar^2}, D = \frac{2\mu k_0}{\hbar^2},, \quad \gamma = l(l+1)\Big\}. \tag{15}$$

Equation (14) contains terms of order ${x_d}^3$ *and* ${x_d}^4$. To simplify and obtain an approximate analytical solution, we neglect these terms by assuming to $\alpha r_q \prec 1$ [30]. Truncation of higher-order terms simplifies mathematical models, making them more computationally efficient while retaining physically realistic outcomes. This approach reduces complexity, enhances interpretability, and enables practical application in systems where lower-order terms dominate, ensuring accurate predictions without unnecessary computational overhead, especially in well-defined parameter regimes with minimal influence from higher-order contributions. Consequently, Eq. (14) reduces to

$$\frac{d^2\psi(x_d)}{dx_d{}^2} + \frac{1-x_d}{x_d(1-x_d)}\frac{d\psi(x_d)}{dx_d} + \frac{1}{[x_d(1-x_d)]^2}\begin{bmatrix} -(\varepsilon + 6A + 3B){x_d}^2 \\ +(2\varepsilon + 4A + 3B - C)x_d \\ -(\varepsilon + A + B - C + D + \gamma) \end{bmatrix}\psi(x_d) = 0, \tag{16}$$

The comparison of Eq. (16) and Eq. (A1) of Appendix A, the following polynomials are gotten;

$$\begin{aligned} &\tilde{\tau}(x_d) = 1 - x_d;\ \sigma(x_d) = x_d(1-x_d);\ \sigma'(x_d) = 1 - 2x_d, \\ &\sigma''(x_d) = -2; \sigma(x_d) = -(\varepsilon + 6A + 3B){x_d}^2 \\ &+(2\varepsilon + 4A + 3B - C)x_d - (\varepsilon + A + B - C + D + \gamma) \end{aligned} \tag{17}$$

Inserting the polynomials given into Eq. (A9) of Appendix A, gives

$$\pi(x_d) = -\frac{x_d}{2} \pm \sqrt{(A_1 - K){x_d}^2 + (K + A_2)x_d + A_3},$$

where

$$A_1 = \left(\frac{1}{4} + \varepsilon + 6A + 3B\right), \quad A_2 = -(2\varepsilon + 4A + 3B - C), \quad A_3 = (\varepsilon + A + B - C + D + \gamma).$$

The NU method stipulates that the discriminant of the quadratic equation must be equal to zero. By using the discriminant, we can solve for the constant k to determine the two roots. In this particular analysis, we concentrate on the negative square root, expressed as:

$$K = -(A_2 + 2A_3) - 2\sqrt{A_3}\sqrt{A_3 + A_2 + A_1}. \tag{18}$$

We then put Eq. (18) into $\pi(x_d) = -\frac{x_d}{2} \pm \sqrt{(A_1 - K){x_d}^2 + (K + A_2)x_d + A_3}$, and obtain, $\pi(x_d)$has the most suitable expression given as

$$\pi(x_d) = -\frac{x_d}{2} - \left[\left(\sqrt{A_3} + \sqrt{A_3 + A_2 + A_1}\right)x_d - \sqrt{A_3}\right], \tag{19}$$

Using the polynomials and Eq. (17). Therefore, we obtain $\tau(x_d)$ and $\tau^{/}(x_d)$ as follows:

$$\tau(x_d) = 1 - 2x_d - 2\sqrt{A_3}x_d - 2\sqrt{A_3 + A_2 + A_1}x_d + 2\sqrt{A_3}, \tag{20}$$

$$\tau^{/}(x_d) = -2\left[1 + \sqrt{A_3} + \sqrt{A_3 + A_2 + A_1}\right],. \tag{21}$$

Referring to Eq. (A10) and Eq. (A11) of Appendix A, the following expressions for λ_n and λ are as follows:

$$\lambda_n = n^2 + \left[1 + 2\sqrt{A_3} + 2\sqrt{A_3 + A_2 + A_1}\right]n, (n = 0,1,2,\dots), \tag{22}$$

$$\lambda = -\frac{1}{2} - \sqrt{A_3} - \sqrt{A_3 + A_2 + A_1} - (A_2 + 2A_3) - 2\sqrt{A_3}\sqrt{A_3 + A_2 + A_1}, \tag{23}$$

The eigenvalues of the RSPP is obtained by equating Eqs. (22) and (23) and incorporating Eq. (15)

$$E_{nl} = \frac{\alpha^2\hbar^2 l(l+1)}{2\mu} + \frac{a_0}{\alpha^2} - \alpha g_0 + \alpha^2 k_0 + d_0 + b_0 - \frac{\alpha^2\hbar^2}{8\mu}\left[\frac{\left(n+\frac{1}{2}+\sqrt{\left(l+\frac{1}{2}\right)^2+\frac{6\mu a_0}{\alpha^4\hbar^2}+\frac{2\mu b_0}{\alpha^3\hbar^2}+\frac{2\mu k_0}{\hbar^2}}\right)^2 - \frac{4\mu a_0}{\alpha^4\hbar^2} - \frac{2\mu b_0}{\alpha^3\hbar^2} - \frac{2\mu g_0}{\alpha\hbar^2} + \frac{4\mu k_0}{\hbar^2} + l(l+1)}{n+\frac{1}{2}+\sqrt{\left(l+\frac{1}{2}\right)^2+\frac{6\mu a_0}{\alpha^4\hbar^2}+\frac{2\mu b_0}{\alpha^3\hbar^2}+\frac{2\mu k_0}{\hbar^2}}}\right]^2 \tag{24}$$

The derivation of energy eigenvalues in Eq. (24) follows a precise and methodical approach, incorporating standard approximation techniques and ensuring mathematical rigor. It systematically applies boundary conditions, and potential terms, yielding results that align with established theory. The derivation effectively captures essential physical behavior while maintaining mathematical consistency.

The wave function (WF) for the ground state and the first excited state, along with their normalization constants, are presented in Eqs. (25) and (26).

$$\psi_{0l}\left(r_q\right) = \sqrt{\frac{\alpha\,\Gamma\,[2(1+A+B)]}{\Gamma\,[2A]\,\Gamma\,[2+2B]}} \times (e^{-\alpha\, r_q})^A \times (1 - e^{-\alpha\, r_q})^{B+\frac{1}{2}} \tag{25}$$

$$\psi_{1l}\left(r_q\right) = \sqrt{\frac{2A(3+2A+2B)\alpha\,\Gamma\,[2(1+A+B)]}{(3+2B)\,\Gamma\,[2+2A]\,\Gamma\,[2+2B]}} \times \left(e^{-\alpha\, r_q}\right)^A \times (1 - e^{-\alpha\, r_q})^{B+\frac{1}{2}} \times \mathrm{P}_1^{(2A,2B)}\left(1 - 2e^{-\alpha\, r_q}\right), \tag{26}$$

where

$$A = \sqrt{l \times (l+1) - \frac{2m}{\alpha^2\hbar^2} \times (E_{nl} - a) - \frac{2m}{\alpha^2\hbar^2}}; \quad B = l + \frac{1}{2}$$

P_1 and Γ are Jacobi and Gamma functions respectively

The wave function in momentum space is expressed as

$$\Psi_{00}(p) = \sqrt{\frac{1}{2\pi}}\sqrt{\frac{\alpha\,\Gamma\,[2(1+A+B)]}{\Gamma\,[2A]\,\Gamma\,[2+2B]}}\int_0^\infty (e^{-\alpha\, r_q})^A \times (1 - e^{-\alpha\, r_q})^{B+\frac{1}{2}} e^{-ip\, r_q}\, d\, r_q \tag{27}$$

$$\Psi_{00}(p) = \sqrt{\frac{\alpha\,\Gamma\,[2(1+A+B)]}{\Gamma\,[2A]\,\Gamma\,[2+2B]}} \times \frac{\Gamma\,[\frac{3}{2}+B]\,\Gamma\,[A+\frac{ip}{\alpha}]}{\sqrt{2\pi}\alpha\,\Gamma\,[\frac{3}{2}+A+B+\frac{ip}{\alpha}]} \quad . \tag{28}$$

The eigenfunction corresponding to the SE in spherical polar coordinates is expressed as:

.

$$\Psi_{nlm}\left(r_q,\theta_{r_q},\phi_{r_q}\right)=\frac{R_{nl}\left(r_q\right)}{r_q}Y_{lm}\left(\theta_{r_q},\phi_{r_q}\right). \tag{29}$$

The spherical harmonics $Y_{lm}(\theta,\phi)$ is defined by

$$Y_{lm}(\theta,\phi)=(-1)^m\sqrt{\frac{2l+1(l-m)!}{4\pi(l+m)!}}P_l^m(\cos\theta)e^{im\phi} \tag{30}$$

where the function $P_l^m(Cos\theta)$ is the associated Legendre function.

The wave function in momentum space is represented by the Fourier transform [31].

$$\Psi_{nlm}(p,\theta_p,\phi_p)=\frac{1}{(2\pi)^{3/2}}\int_{\mathbb{R}^3}\Psi_{nlm}\left(r_q,\theta_{r_q},\phi_{r_q}\right)e^{-i\bar{p}.\bar{r}}\,d^{\,3}r_q \tag{31}$$

The notation $d^{\,3}r_q=\left(r_q^{\,2}dr_q\right)sin\theta d\theta d\phi$ is the volume element. The plane-wave expansion for $e^{-i\bar{p}.\overline{r_q}}$ is given as

$$e^{-i\bar{p}.\overline{r_q}}=(2\pi)^{3/2}\sum_{l=0}^{\infty}\sum_{m=-l}^{l}i^{-l}\frac{J_{l+1/2}\left(p\,r_q\right)}{\sqrt{p\,r_q}}\,\mathrm{Y}_{lm}(\theta_p,\phi_p)\mathrm{Y}_{lm}^{*}\left(\theta_{r_q},\phi_{r_q}\right)\ [32] \tag{32}$$

Given the axial symmetry, only the m = 0 terms remain, which simplifies the plane-wave expansion significantly.

$$e^{-i\bar{p}.\overline{r_q}}=(2\pi)^{3/2}\mathrm{Y}_{lm}(\theta_p,\phi_p)\sum_{l=0}^{\infty}i^{-l}\frac{J_{l+1/2}\left(p\,r_q\right)}{\sqrt{p\,r_q}}\,\mathrm{Y}_{l0}^{*}\left(\theta_{r_q},\phi_{r_q}\right) \tag{33}$$

Substituting equations (30) and (33) into equation (32) yields

$$\Psi_{nlm}(p,\theta_p,\phi_p)=i^{-l}\mathrm{Y}_{lm}(\theta_p,\phi_p)\int_0^{\pi}\int_0^{2\pi}\mathrm{Y}_{l0}\left(\theta_{r_q},\phi_{r_q}\right)\mathrm{Y}_{l0}^{*}\left(\theta_{r_q},\phi_{r_q}\right)sin\theta d\theta d\phi$$
$$\times\int_0^{\infty}\frac{R_{nl}\left(r_q\right)}{r_q}\,\frac{J_{l+1/2}\left(p\,r_q\right)}{\sqrt{p\,r_q}}\,r_q^{\,2}dr_q \tag{34}$$

For the ground state, the orthonormality condition of the spherical harmonics is applied to simplify the analysis.

$$\Psi_{000}(p,\theta_p,\phi_p)=\frac{\mathrm{Y}_{00}(\theta_p,\ \phi_p)}{\sqrt{p}}F_{00}(p) \tag{35}$$

where,

$$F_{00}(p)=\int_0^{\infty}\sqrt{r_q}R_{00}\left(r_q\right)J_{1/2}\left(p\,r_q\right)dr_q \tag{36}$$

The momentum space wave function is obtained using MATHEMATICA software, as given by:

$$\Psi_{000}(p,\theta_p,\phi_p)=\frac{(-1)^{1/4}e^{-\frac{i\pi}{4}}\Gamma\left[\frac{3}{2}+B\right]\sqrt{\frac{\alpha\,\Gamma\,[2(1+A+B)]}{\Gamma\,[2A]\,\Gamma\,[2+2B]}}\left(-\frac{i\,\Gamma\,[A-\frac{ip}{\alpha}]}{\Gamma\,[\frac{3}{2}+A+B-\frac{ip}{\alpha}]}+\frac{i\,\Gamma\,\mathrm{a}[A+\frac{ip}{\alpha}]}{\Gamma\,[\frac{3}{2}+A+B+\frac{ip}{\alpha}]}\right)}{p\sqrt{2\pi\alpha}}\mathrm{Y}_{00}(\theta_p,\ \phi_p) \tag{37}$$

2.1 Oscillator Strength

Oscillator strength is a dimensionless quantity that represents the probability of a system, like an atom or molecule, absorbing or emitting electromagnetic radiation. It represents the intensity of transitions between energy states, with higher values corresponding to more significant transitions. This parameter is crucial for analyzing spectra and atomic/molecular interactions. The expression is given by:

$$f_{ij}^{l} = \frac{2M}{3\hbar^2}\left(E_j - E_i\right)\left|\langle\psi_j|r|\psi_i\rangle\right|^2 \tag{38}$$

where $E_j \; and \; \psi_j$are at a higher state than the respective $E_i \; and \; \psi_i$. The M represents an electronic mass. The notation $\left|\langle\psi_j|r|\psi_i\rangle\right|$ is the matrix element and $\left(E_j - E_i\right)$is the energy difference [19].

2.2. Expectation values and the Heisenberg Uncertainty principle

The expression for the expectation value (EV) of $\boldsymbol{r_q}$, $\boldsymbol{r_q}^{\boldsymbol{2}}$, and $\hat{\boldsymbol{p}}^{\boldsymbol{2}}$are as follows [1].

$$\langle r_q\rangle_n = \int_0^\infty R_{n\ell} r_q R_{.n\ell}\, dr_q \tag{39}$$

$$\langle {r_q}^2\rangle_n = \int_0^\infty R_{.n\ell} {r_q}^2 R_{n\ell} dr_q \tag{40}$$

$$\langle\hat{p}^2\rangle_n = \int_0^\infty R_{n\ell}\hat{p}^2 R_{.n\ell} dr_q = \; -\int_0^\infty R_{nl}(r)\frac{d^2}{dr_q^2} R_{n.l}^{*}(r) dr_q \tag{41}$$

The uncertainties in both position and momentum are evaluated using Equations (42) and (43) [1].

$$\Delta r_q = \sqrt{\langle r_q^2\rangle - \langle r_q\rangle^2} \tag{42}$$

$$\Delta p = \sqrt{\langle p^2\rangle - \langle p\rangle^2} \tag{43}$$

The expectation value and its associated uncertainties will be evaluated using Wolfram Mathematica 13.

3. Case Study: Diatomic Molecules

Formed through the covalent bonding of two atoms, diatomic molecules are fundamental to numerous physical and chemical phenomena. Their importance spans diverse fields, from atmospheric chemistry to molecular spectroscopy and quantum mechanical modeling. Recent studies [2,24-26,33] have significantly enriched our understanding of their intrinsic properties, providing advanced theoretical models and experimental data that offer deeper insights into their structure, dynamics, and interactions. The potential utilized in our study enables the investigation of diatomic molecules by setting $g_0 = 2D_e r_e, k_0 = D_e r_e^2, a_0 = b_0 = d_0 = 0$ of Eq. (12), we have the Kratzer potential and the energy equation is given as Eq.(44), when $\alpha = 0$. The Kratzer potential has emerged as a key model in atomic and molecular physics, particularly in the study of vibrational and rotational spectroscopy [34]. Its relevance in molecular physics is both substantial and widely acknowledged.

$$E_{nl} = -\frac{2\mu_a}{\hbar^2} D_e^2 r_e^2 \left[n + \frac{1}{2} + \sqrt{\left(l + \frac{1}{2}\right)^2 + \frac{2\mu_a D_e r_e^2}{\hbar^2}}\right]^{-2} \tag{44}$$

4. Results and Discussion

The NU method was employed to derive the energy spectrum of the Schrödinger equation under the RSPP, retaining terms up to the second order. This approximation ensures accuracy in position space, which is critical because information-theoretic measures such as Fisher information, Shannon entropy, and Rényi entropy are highly sensitive to the precision of the underlying wavefunctions. Fisher information, which characterizes the localization or sharpness of a probability distribution, responds strongly to even minor variations in eigenvalues. Similarly, Shannon and Rényi entropies, which quantify the uncertainty and spread of quantum states, are directly influenced by the accuracy of the eigenfunctions and their corresponding spectra. Consequently, enhancing the precision of eigenvalue approximations significantly improves the reliability and fidelity of these entropy-based analyses in both coordinate and momentum representations, offering deeper insights into the fundamental behavior of quantum systems. Table 1 reports the one-dimensional ground-state Shannon entropy for various values of the screening parameter α. As α increases, entropy in position space rises, while it decreases in momentum space, illustrating the trade-off between

.

precision in conjugate variables and confirming compliance with the BBM inequality. A similar pattern is observed in Table 2, which presents the three-dimensional ground-state Shannon entropy over the range α=0.01to 0.09. In all cases, the total entropy exceeds the BBM bound of 6.4343, reaffirming the fundamental quantum constraint on simultaneous measurements of position and momentum.

Table 1. Numerical Values of Position and Momentum Shannon Entropies for the One-Dimensional Ground State using parameters $a_0, = 1.9, b_0 = 1.7, d_0 = 1.8, g_0 = 1.1, k_0 = 0.02, \mu = 1, \hbar = 1$

α	$S(\rho)$	$S(\gamma)$	$S(\rho) + S(\gamma) \geq 2.14473$
0.01	2.014582633	0.130538251	2.145120884
0.02	2.017227462	0.129000744	2.146228206
0.03	2.016882987	0.12872739	2.145610377
0.04	2.024335028	0.121969552	2.14630458
0.05	2.038506689	0.108715548	2.147222237
0.06	2.061039402	0.087358576	2.148397978
0.07	2.093779221	0.05611188	2.149891102
0.08	2.138926224	0.012875116	2.15180134
0.09	2.199166310	-0.044868907	2.154297403

Table 2. Numerical Values of Position and Momentum Shannon Entropies for the three-dimensional Ground State using parameters $a_0, = 1.9, b_0 = 1.7, d_0 = 1.8, g_0 = 1.1, k_0 = 0.02, \mu = 1, \hbar = 1$

α	$S(\rho)$	$S(\gamma)$	$S(\rho) + S(\gamma) \geq 6.4342$
0.01	2.356488661	4.210105084	6.566593745
0.02	0.127911327	6.438681244	6.566592571
0.03	-1.136590993	7.703183368	6.566592375
0.04	-2.023404187	6.058972249	4.035568062
0.05	-2.707005078	9.273597358	6.566592279
0.06	-3.263379488	9.829971751	6.566592263
0.07	-3.732534727	10.29912698	6.566592253
0.08	-4.138146485	10.70473873	6.566592247
0.09	-4.495392354	11.06198460	6.566592243

Table 3 displays the one-dimensional ground-state Fisher information for various values of α. As expected, the product of Fisher information in position and momentum spaces satisfies the SCR inequality. Increasing α enhances position-space Fisher information reflecting improved localization while reducing momentum-space information, demonstrating the intrinsic limits imposed by the uncertainty principle.

Table 3. Numerical Values of Position and Momentum Fisher Information for the One-Dimensional Ground State using parameters $a_0, = 1.9, b_0 = 1.7, d_0 = 1.8, g_0 = 1.1, k_0 = 0.02, \mu = 1, \hbar = 1$

α	$I(\rho)$	$I(\gamma)$	$I(\rho)I(\gamma) \geq 4$
0.01	0.30313370	13.19549806	4.000000150
0.02	0.30406752	13.1550108	4.000011510
0.03	0.302969164	13.20285708	4.000058572
0.04	0.298904296	13.38283435	4.000186677
0.05	0.291090195	13.74304620	4.000466004
0.06	0.278928026	14.34422399	4.001006078
0.07	0.262046936	15.27201902	4.001985792
0.08	0.240366064	16.65674436	4.003716087
0.09	0.214192951	18.70638388	4.006775559

This inverse relationship persists in three dimensions, as shown in Table 4. As α increases, position-space Fisher information becomes more pronounced, indicating sharper localization, whereas momentum-space information decreases. These trends not only comply with the SCR inequality but also highlight how α influences the fundamental trade-off between precision in conjugate observables.

Table 5 presents numerically computed Rényi entropies for the index parameter q=0.5. The data show that increasing α leads to higher entropy in both coordinate and momentum spaces, emphasizing the role of screening in enhancing the system's overall uncertainty.

Table 4. Numerical Values of Position and Momentum Fisher Information for the three-Dimensional Ground State using parameters $a_0, = 1.9, b_0 = 1.7, d_0 = 1.8, g_0 = 1.1, k_0 = 0.02, \mu = 1, \hbar = 1$

α	$I(\rho)$	$I(\gamma)$	$I(\rho)I(\gamma) \geq 36$
0.01	13.1768	3.642751741	47.99981114
0.02	58.2168	0.824488281	47.99906934
0.03	135.2568	0.354872211	47.99887971
0.04	244.2968	0.196477482	47.99882003
0.05	385.3368	0.124563430	47.99887357
0.06	558.3768	0.085961509	47.99891224
0.07	763.4168	0.062873883	47.99897888
0.08	1000.4568	0.047977061	47.99897643
0.09	1269.4968	0.037809514	47.99905749

Table 5. Numerical Values of Position and Momentum Renyi information using parameters $a_0, = 1.9, b_0 = 1.7, d_0 = 1.8, g_0 = 1.1, k_0 = 0.02, \mu = 1, \hbar = 1$

α	$R_{0.6}(\rho)$	$R_3(\gamma)$	$R_{0.6}(\rho) + R_3(\gamma) \geq 2.057915$
0.01	2.017227462	-0.096433416	2.057944483
0.02	2.014582633	-0.095156679	2.058045411
0.03	2.016882987	-0.097403422	2.058208962
0.04	2.024335028	-0.104780595	2.058441418
0.05	2.038506689	-0.118856345	2.058749655
0.06	2.061039402	-0.141272364	2.059146266
0.07	2.093779221	-0.173875004	2.05965288
0.08	2.138926224	-0.218864514	2.060306226
0.09	2.19916631	-0.278926653	2.061169497

Furthermore, as the index q increases, Rényi entropy also rises, confirming its sensitivity to the shape of the underlying probability distribution. This behavior supports the use of Rényi entropy as a generalized measure for exploring quantum delocalization, coherence, and complexity. In Table 6, the expectation values ⟨r⟩, ⟨r^2⟩, and ⟨p^2⟩ are reported for the ground state. These values provide additional insight into the average behavior of quantum observables and reinforce the Heisenberg Uncertainty Principle by illustrating the inherent limits on the simultaneous accuracy of position and momentum measurements.

Table. 6: Numerical Values of Expectation values and Heisenberg uncertainty using parameters $a_0, = 1.9, b_0 = 1.7, d_0 = 1.8, g_0 = 1.1, k_0 = 0.02, \mu = 1, \hbar = 1$

α	$\langle r \rangle$	$\langle r^2 \rangle$	$\langle p^2 \rangle$	$\Delta r \Delta p \geq 0.5$
0.01	194.1635691	37702.79139	0.075783437	0.500073000
0.02	97.02067465	9416.303916	0.076016882	0.500293610
0.03	64.82897404	4206.10529	0.075742291	0.500662210
0.04	48.93699129	2398.190572	0.074726074	0.501186938
0.05	39.6153286	1572.835561	0.072772549	0.501884149
0.06	33.62556095	1134.303532	0.069732006	0.502783536
0.07	29.58801336	879.3269599	0.065511734	0.503935848
0.08	26.82459241	723.8098833	0.060091516	0.505427125
0.09	24.97346852	628.4821408	0.053548238	0.507405668

Table 7 shows that, as α increases, oscillator strengths decrease. This decline reflects reduced interaction between the electric field and electronic states, leading to lower transition probabilities. These trends are consistent with previous studies using other potential models, highlighting the robustness of the observed behavior.

.

Table. 7: Numerical Values of Oscillator Strength for the Radial Scalar Power Potential, using parameters $a_0, = -20, b_0 = 3, d_0 = 4.8, g_0 = 2, k_0 = 1, \mu = 1, \hbar = 1$

Transition	α	f_{ij}^{l}
1s – 2p	0.0250	150.7654321
	0.0500	149.8765432
	0.0750	148.9876543
	0.1000	148.0987654
	0.1500	147.2098765
1s – 3p	0.0250	2900.123456
	0.0500	1450.234567
	0.0750	950.3456789
	0.1000	710.4567890
	0.1500	460.5678901

By imposing specific boundary conditions, the RSPP was reduced to the Kratzer potential, facilitating an accurate analytical treatment. Table 8 summarizes the spectroscopic parameters for CH and N_2 molecules, chosen for their relevance in previous studies and practical applications. Using these parameters in Eq. (44), energy eigenvalues were computed and are presented in Table 9.

Table 8. Spectroscopic properties of the chosen diatomic molecules [35].

Molecules	$D_e(eV)$	$r_e(\dot{A})$	$\mu(amu)$
CH	31838.081490	1.1198	0.929931
N_2	11.938193820	1.0940	7.003350

Table 9: Comparison of bound-state energy (in eV) for different ℓ quantum numbers across various diatomic molecules while keeping n constant.

n	l	CH	CH [40]	N_2	N_2 [40]
0	0	0.083223	0.08322383	0.054436	0.05443655
1	0	0.241150	0.24115051	0.162076	0.16207644
	1	0.244408	0.24440882	0.162565	0.16256502
2	0	0.389589	0.38958988	0.268260	0.26826045
	1	0.392654	0.39265445	0.268742	0.26874244
	2	0.398767	0.39876758	0.269706	0.26970629
3	0	0.529286	0.52928690	0.373014	0.37301474
	1	0.532172	0.53217281	0.373490	0.37349025
	2	0.537929	0.53792974	0.374441	0.37444116
	3	0.546528	0.54652818	0.375867	0.37586721
4	0	0.660914	0.66091486	0.476364	0.47636485
	1	0.663635	0.66363571	0.476834	0.47683401
	2	0.669063	0.66906360	0.477772	0.47777219
	3	0.677171	0.67717107	0.479179	0.47917917
	4	0.687917	0.68791738	0.481054	0.48105461
5	0	0.785083	0.78508342	0.578335	0.57833578
	1	0.787651	0.78765158	0.578798	0.57879869
	2	0.792775	0.79277502	0.579724	0.57972438
	3	0.800428	0.80042821	0.581112	0.58111263
	4	0.810573	0.81057320	0.582963	0.58296310
	5	0.823160	0.82316019	0.585275	0.58527534

The results show strong agreement with alternative analytical methods [35]. For a fixed principal quantum number n, increasing the angular momentum quantum number ℓ leads to higher energy levels, reflecting the

centrifugal contribution to the effective potential and its implications for molecular stability and spectroscopic behavior. Beyond the Kratzer limit, the full RSPP model reveals deeper physical trends. The results show that the screening parameter directly affects the spatial confinement of the system. Stronger screening leads to more localized wavefunctions, larger energy spacings, and reduced overlap between states, which lowers oscillator strengths and reduces transition probabilities. These changes are reflected in information-theoretic measures as well, with Fisher information increasing in position space and Shannon and Rényi entropies capturing the redistribution of uncertainty between conjugate variables. These results demonstrate that the potential shape influences measurable spectroscopic properties and the quantum information content of the states, highlighting the practical significance of our findings for understanding and predicting transition behaviors in the system.

Figures 1(a) and 1(b) illustrate wavefunction profiles and corresponding probability densities for ℓ=1. As n increases, wavefunctions become more oscillatory, with higher amplitudes and additional nodes, indicating the emergence of distinct quantum states. The associated probability densities display Gaussian-like peaks, supporting the quantized nature of the system and confirming compliance with the BBM inequality. Figures 2(a) and 2(b) extend this analysis to ℓ=2, further confirming the influence of the potential on wavefunction structure and spatial localization.

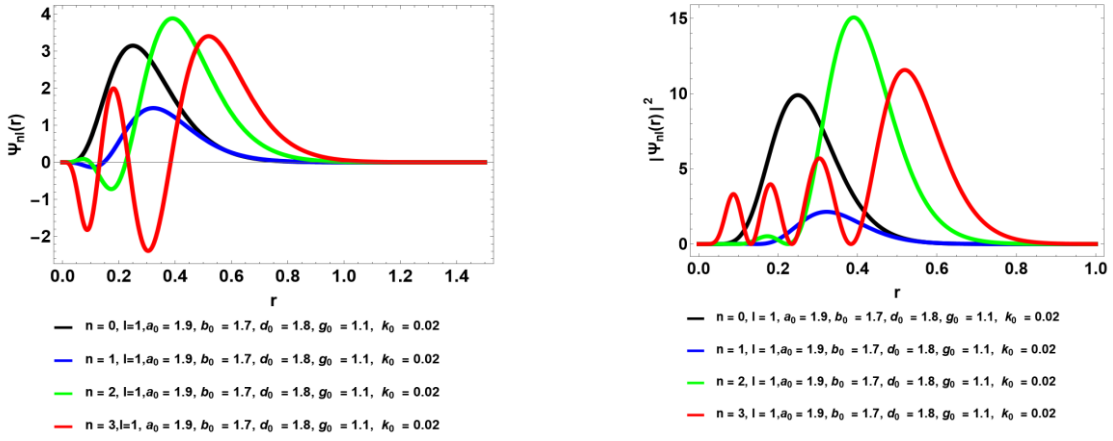

a) b)

Fig.1. *(a)* Radial wave functions and *(b)* corresponding probability density functions for various principal quantum numbers n, at l =1

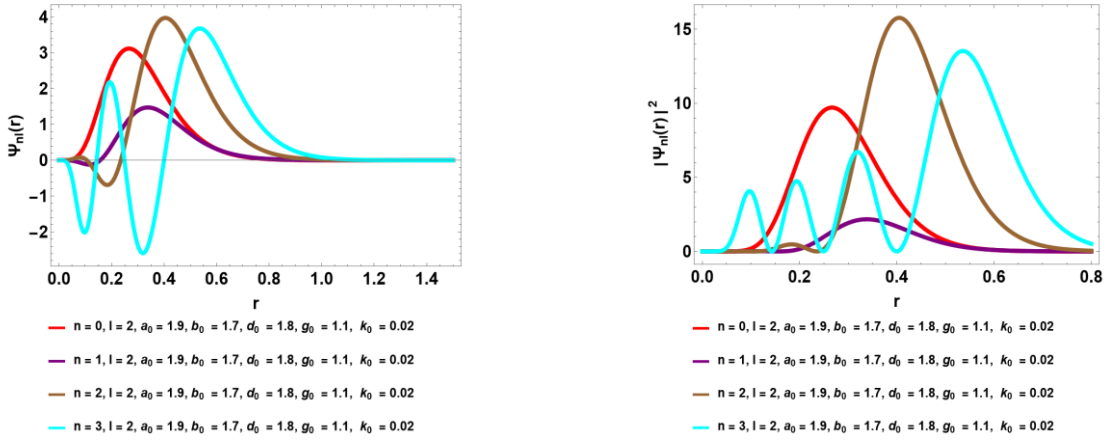

a) b)

Fig. 2. *(a)* Radial wave functions and *(b)* corresponding probability density functions for various principal quantum numbers, at l =2

Figures 3(a) and 3(b) show the variation of Shannon entropy with respect to α. An increase in α leads to a decline in position-space entropy and a corresponding rise in momentum-space entropy, reinforcing the uncertainty principle.

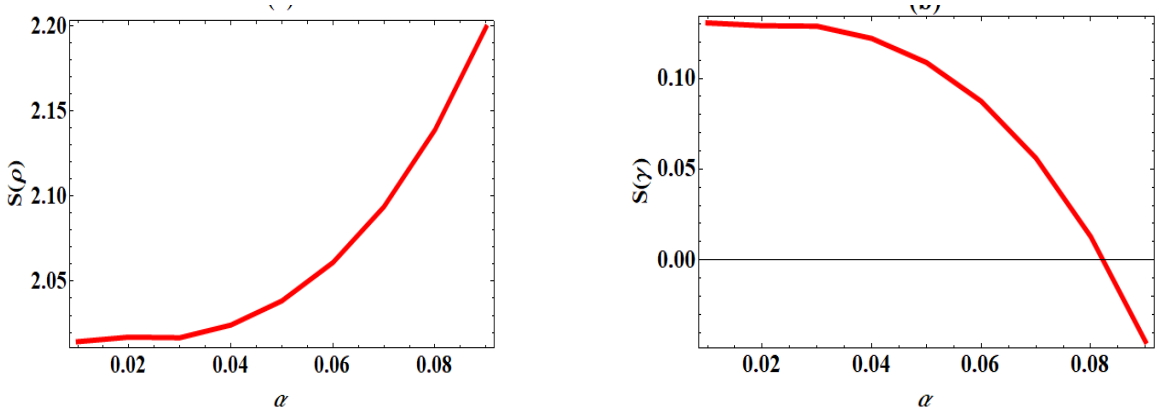

a) b)

Fig 3. (a, b): Variations of Shannon entropies with α parameter

Figures 4(a) and 4(b) depict Fisher information under the same variation. As α increases, Fisher information in position space rises, signifying enhanced sensitivity to parameter changes, while it declines in momentum space, reflecting decreased sensitivity in that domain. Finally, Figures 5(a) and 5(b) illustrate Rényi entropy trends with respect to α. As α increases, Rényi entropy decreases in momentum space while increasing in position space. This duality highlights the system's evolving structure and localization as a function of the screening parameter.

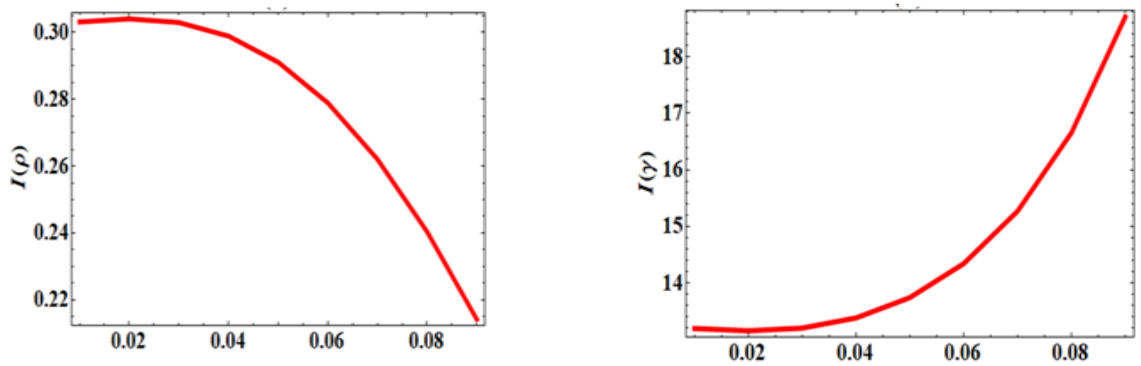

a) b)

Fig. 4. (a, b): Variations of Fisher information with α parameter

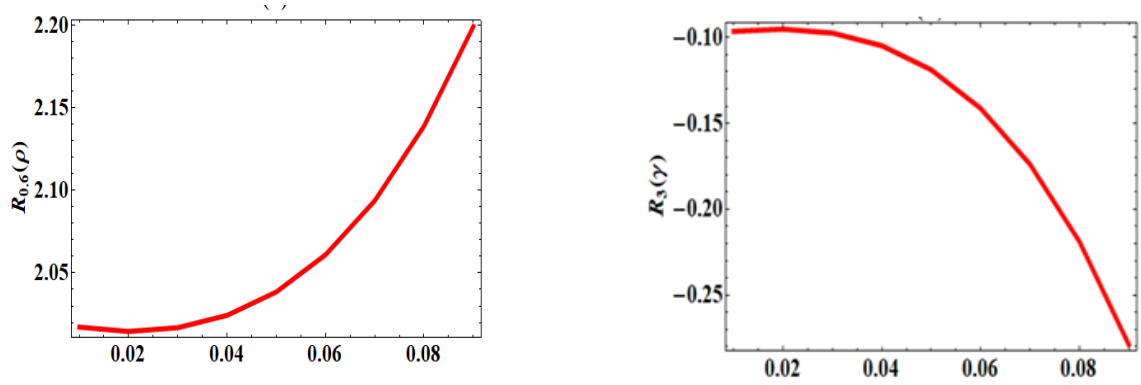

a) b)

Fig. 5. (a, b): Variations of Renyi entropy with α parameter

These complementary behaviors in position and momentum representations are in full agreement with the uncertainty principle, illustrating the balance between information content in conjugate domains. This integrated analysis not only reinforces the foundational constraints of quantum mechanics but also enhances

our understanding of how information is distributed between conjugate variables, providing valuable insights for quantum measurement, coherence, and the design of quantum technologies.

5. Conclusions

In this study, the Schrödinger equation for the Radial Scalar Power Potential (RSPP) was solved analytically using the NU method, applying the Greene–Aldrich approximation and an appropriate coordinate transformation. This allowed us to obtain energy eigenvalues and normalized wavefunctions, which were then used to compute expectation values, Shannon entropy, Fisher information, Rényi entropy, and oscillator strengths in both position and momentum spaces.

Our results confirm that Shannon entropy and Fisher information satisfy the BBM and SCR inequalities in one- and three-dimensional cases, reaffirming the quantum mechanical limits on the simultaneous precision of conjugate observables. Wavefunction and probability density analyses for $\ell=1$ and $\ell=2$ demonstrate an inverse behavior of Fisher information: increases in one space correspond to decreases in the other, reflecting the uncertainty equilibrium inherent in quantum systems.

By imposing specific boundary conditions, the RSPP reduces to the Kratzer potential, enabling accurate computation of energy eigenvalues for methylidyne (CH) and nitrogen (N_2) molecules. Energy levels rise with increasing angular momentum quantum number, highlighting the centrifugal contribution to the effective potential and its relevance for molecular stability and spectroscopic transitions. Additionally, oscillator strengths decrease with higher screening parameters, indicating reduced electron–field interaction and lower transition probabilities, in agreement with prior studies. These findings provide a clear physical interpretation of the relationships between potential parameters, wavefunction localization, and information-theoretic measures. They emphasize the connection between quantum uncertainty and measurable quantities, such as transition energies and oscillator strengths. The results have practical implications for molecular spectroscopy, modeling of diatomic systems, and the design of quantum sensors, offering a framework for further exploration in quantum information theory and related technological applications.

Conflict of interest statement

The authors declare that they have **no conflict of interest** in relation to this research, whether financial, personal, authorship or otherwise, that could affect the research and its results presented in this paper.

CRediT author statement

Inyang E.P.: Conceptualization, Methodology, Writing-Original draft preparation, Funding acquisition; **Nwachukwu I. M.**: Software Funding acquisition; **Okoi P.O.**: Visualization, Validation, Funding acquisition. The final manuscript was read and approved by all authors.

Funding

This research was supported by the 2025 Senate Research Grant from the National Open University of Nigeria: with grant number NOUN/DRA/SRG/AW/035.

Acknowledgements

The authors, expresses appreciation to the National Open University of Nigeria for the 2025 Senate Research Grant.

References

1 Inyang E.P., Omugbe E., Abu-shady M., William E.S. (2023) Investigation of quantum information theory with the screened modified Kratzer and a class of Yukawa potential model. *Eur Phys J Plus*, 138 (11), 969. https://doi.org/10.1140/epjp/s13360-023-04617-7

2 Inyang E. P. (2025) Quantum expectation values and Shannon entropy in diatomic molecular systems. *Journal of Mathematical Chemistry*. https://doi.org/10.1007/s10910-025-01738-5

3 Inyang E.P., Aouami A.E.L., Ali N., Endut R., Ali N.R., Aljunid S.A. (2024) Information entropies with Varshni-Hellmann potential in higher dimensions. *Phys Open*, 100220. https://doi.org/10.1016/j.physo.2024.100220

4 Dong S., Sun G.H., Dong S.H., Draayer J.P. (2014) Quantum information entropies for a squared tangent potential well. *Phys Lett A*, 378(3), 124–130. https://doi.org/10.1016/j.physleta.2013.11.020

5 Pooja, Kumar R., Kumar G., Kumar R., Kumar A. (2016) Quantum information entropy of Eckart potential. *Int J Quantum Chem*, 116(19), 1413–1418. https://doi.org/10.1002/qua.25197

.

6 Heisenberg W. (1927) Über den anschaulichen Inhalt der quantentheoretischen Kinematik und Mechanik. *Z Phys*, 43, 172–198. https://doi.org/10.1007/BF01397280

7 Białynicki-Birula I., Mycielski J. (1975) Uncertainty relations for information entropy in wave mechanics. *Commun Math Phys*, 44, 129–132. https://doi.org/10.1007/BF01608825

8 Hirschman I.I. (1957) A note on entropy. *Am J Math*, 79(1), 152–156. https://doi.org/10.2307/2372390

9 Beckner W. (1975) Inequalities in Fourier analysis. *Ann Math*, 102(1):159–182. https://doi.org/10.2307/1970980

10 Esquivel Olea R.O., Molina Espíritu M., López Rosa S. (2023) 3D information-theoretic analysis of the simplest hydrogen abstraction reaction. *J Phys Chem A*,127(30), 6159–6174. https://doi.org/10.1021/acs.jpca.3c01957

11 Omugbe E., Osafile O.E., Okon I.B., Eyube E.S., Inyang E.P., Okorie U.S., Onate C.A. (2022) Non-relativistic bound state solutions with α-deformed Kratzer-type potential using the supersymmetric WKB method: Application to theoretic-information measures. *Eur Phys J D*, 76(4), 72. https://doi.org/10.1140/epjd/s10053-022-00395-6

12 Rényi A. (1960) On measures of information theory. In: Neyman J., ed. *Proc 4th Berkeley Symp Math Stat Probab*, I, 547–561. Berkeley, CA: Berkeley Univ. Press.

13 Njoku I.J., Onyenegecha C.P. (2024) Global and local information-theoretic measures of the inversely quadratic Hellmann–Kratzer potential. *Chin J Phys*, 88, 594–608. https://doi.org/10.1016/j.cjph.2023.10.014

14 Amadi P.O., Ikot A.N., Rampho G.J., Okorie U.S., Abdullah H.Y., Lütfüoğlu B.C. (2020) Information entropies for H_2 and ScF diatomic molecules with Deng-Fan-Eckart potential. *Rev Mex Fis*; 66(6), 742–748. https://doi.org/10.31349/revmexfis.66.742

15 Onyeaju M.C., Omugbe E., Onate C.A., Okon I.B., Eyube E.S., Okorie U.S., et al. (2023) Information theory and thermodynamic properties of diatomic molecules using molecular potential. *J Mol Model*, 29(10), 311. https://doi.org/10.1007/s00894-023-05708-z

16 Laguna H.G., Salazar S.J., Sagar R.P. (2022) Information theoretical statistical discrimination measures for electronic densities. *J Math Chem*, 60(7), 1422–1444. https://doi.org/10.1007/s10910-022-01363-6

17 Njoku I.J., Onyeocha E., Onyenegecha C.P., Onuoha M., Egeonu E.K., Nwaokafor P. (2023) Quantum information of the modified Mobius squared plus Eckart potential. *Int J Quantum Chem*, 123(6), e27050. https://doi.org/10.1002/qua.27050

18 Estañón C.R., Montgomery H.E. Jr, Angulo J.C., Aquino N. (2024) The confined helium atom: An information–theoretic approach. *Int J Quantum Chem*, 124(4), e27358. https://doi.org/10.1002/qua.27358

19 Hibbert A. (1975) Developments in atomic structure calculations. *Rep Prog Phys*, 38(11), 1217. https://doi.org/10.1088/0034-4885/38/11/001

20 Ikot A.N., Hassanabadi H., Obong H.P., Umoren Y.C., Isonguyo C.N., Yazarloo B.H. (2014) Approximate solutions of Klein–Gordon equation with improved Manning–Rosen potential in D-dimensions using SUSYQM. *Chin Phys B*, 23(12), 120303. https://doi.org/10.1088/1674-1056/23/12/120303

21 Varshni Y.P. (1990) Eigenenergies and oscillator strengths for the Hulthén potential. *Phys Rev A*, 41(9), 4682. https://doi.org/10.1103/PhysRevA.41.4682

22 Hassanabadi H., Hoda Y.B., Lu L.L. (2012) Approximate analytical solutions to the generalized Pöschl–Teller potential in D dimensions. *Chin Phys Lett*, 29(2), 020303. https://doi.org/10.1088/0256-307X/29/2/020303

23 Inyang E. P., Nwachukwu I. M., Ekechukwu C.C., Ali N., Lawal K.M. (2025) Variance-based approach to quantum information measures and energy spectra of selected diatomic molecules. *Journal of the Korean Physical Society*. https://doi.org/10.1007/s40042-025-01483-7

24 Inyang E.P., Obisung E.O., Amajama J., Bassey D.E., William E.S., Okon I.B. (2022) The effect of topological defect on the mass spectra of heavy and heavy-light quarkonia. *Eurasian Phys Tech J*, 19(4), 78–87. https://doi.org/10.31489/2022No4/78-87

25 Inyang E.P., Nwachukwu I.M., Ekechukwu C.C., Ekong I.B., William E.S., Lawal K.M., et al. (2024) Analytical solution of the class of inversely quadratic Yukawa potential with application to quantum mechanical systems. *Eurasian Phys Tech J*, 21(4), 118–130. https://doi.org/10.31489/2024No4/118-130

26 Nikiforov S.K., Uvarov V.B. (1988) Special functions of Mathematical Physics, Birkhauser, Basel. Available at: https://link.springer.com/book/10.1007/978-1-4757-1595-8

27 William E.S., Inyang E.P., Thompson E.A. (2020) Arbitrary l-solutions of the Schrödinger equation interacting with Hulthén–Hellmann potential model. *Rev Mex Fis*, 66(6), 730–741. https://doi.org/10.31349/RevMexFis.66.730

28 Inyang E.P., Ali N., Endut R., Rusli N., Aljunid S.A. (2024) The radial scalar power potential and its application to quarkonium systems. *Indian J Phys*, 1–10. https://doi.org/10.1007/s12648-024-03335-9

29 Greene R.L., Aldrich C. (1976) Variational wave functions for a screened Coulomb potential. *Phys Rev A*, 14(6), 2363. https://doi.org/10.1103/PhysRevA.14.2363

30 Tas A., Aydogdu O., Salti M. (2017) Relativistic spinless particles with position dependent mass: Bound states and scattering phase shifts. *J Korean Phys Soc*, 70(10), 896–904. https://doi.org/10.3938/jkps.70.896

31 Kota V.K.B. (2014) *Embedded random matrix ensembles in quantum physics*. Vol. 3, Heidelberg: Springer.

32 Inyang E.P., William E.S., Obu J.O., Ita B.I., Inyang E.P., Akpan I.O. (2021) Energy spectra and expectation values of selected diatomic molecules through the solutions of Klein–Gordon equation with Eckart–Hellmann potential model. *Mol Phys*, 119(23), e1956615. https://doi.org/10.1080/00268976.2021.1956615

33 Inyang E.P., Ali N.R., Aljunid S.A. (2024) Energy spectra, expectation values, and thermodynamic properties of HCl and LiH diatomic molecules. *Eurasian Phys Tech J*; 21, 124–137. https://doi.org/10.31489/2024No1/124-137

34 Inyang E.P., Ntibi J.E., Obisung E.O., William E.S., Ibekwe E.E., Akpan I.O., Inyang E.P. (2022) Expectation values and energy spectra of the Varshni potential in arbitrary dimensions. *Jordan J Phys*, 15(5), 509. https://doi.org/10.47011/15.5.7

35 Rani R., Bhardwaj S.B., Chand F. (2018) Bound state solutions to the Schrödinger equation for some diatomic molecules. *Pramana J Phys*, 91, 46. https://doi.org/10.1007/s12043-018-1622-1

AUTHORS' INFORMATION

Inyang, Etido Patrick – Dr. (Sci.), Department of Physics, Faculty of Science, National Open University of Nigeria, Abuja, Nigeria; ORCID iD: 0000-0002-5031-3297; etidophysics@gmail.com

Okoi, Peter Obeten - Mr. (Sci.), Department of Physics, Faculty of Physical Science, University of Calabar, Calabar, Nigeria; ORCID iD: 0000-0001-9147-425X; okoipeter7@gmail.com

Nwachukwu, Iheke Michael – Dr. (Sci.), Department of Physics, Faculty of Science, National Open University of Nigeria, Abuja, Nigeria; ORCID iD: 0000-0003-2237-7805; inwachukwu@noun.edu.ng

.

APPENDIX A: Review of Nikiforov-Uvarov (NU) method

The NU method was proposed by Nikiforov and Uvarov [31] to transform Schrödinger-like equations into a second-order differential equation via a coordinate transformation $s = s(r)$, of the form

$$\psi''(s) + \frac{\tilde{\tau}(s)}{\sigma(s)}\psi'(s) + \frac{\tilde{\sigma}(s)}{\sigma^2(s)}\psi(s) = 0 \tag{A1}$$

where $\tilde{\sigma}(s)$, and $\sigma(s)$ are polynomials, at most second degree and $\tilde{\tau}(s)$ is a first-degree polynomial. The exact solution of Eq.(A1) can be obtain by using the transformation.

$$\psi(s) = \phi(s)y(s) \tag{A2}$$

This transformation reduces Eq.(A1) into a hypergeometric-type equation of the form

$$\sigma(s)y''(s) + \tau(s)y'(s) + \lambda y(s) = 0 \tag{A3}$$

The function $\phi(x)$ can be defined as the logarithm derivative

$$\frac{\phi'(s)}{\phi(s)} = \frac{\pi(s)}{\sigma(s)} \tag{A4}$$

With $\pi(s)$ being at most a first-degree polynomial. The second part of $\psi(s)$ being $y(s)$ in Eq. (A2) is the hypergeometric function with its polynomial solution given by Rodrigues relation as

$$y(s) = \frac{B_{nl}}{\rho(s)}\frac{d^n}{ds^n}\left[\sigma^n(s)\rho(s)\right] \tag{A5}$$

where B_{nl} is the normalization constant and $\rho(s)$ the weight function which satisfies the condition below;

$$\left(\sigma(s)\rho(s)\right)' = \tau(s)\rho(s) \tag{A6}$$

where also

$$\tau(s) = \tilde{\tau}(s) + 2\pi(s) \tag{A7}$$

For bound solutions, it is required that

$$\tau'(s) < 0 \tag{A8}$$

The eigenfunctions and eigenvalues can be obtained using the definition of the following function $\pi(s)$ and parameter λ, respectively:

$$\pi(s) = \frac{\sigma'(s) - \tilde{\tau}(s)}{2} \pm \sqrt{\left(\frac{\sigma'(s) - \tilde{\tau}(s)}{2}\right)^2 - \tilde{\sigma}(s) + k\sigma(s)} \tag{A9}$$

and

$$\lambda = k_- + \pi_-'(s) \tag{A10}$$

The value of k can be obtained by setting the discriminant in the square root in Eq. (A9) equal to zero. As such, the new eigenvalues equation can be given as

$$\lambda + n\tau'(s) + \frac{n(n-1)}{2}\sigma''(s) = 0, (n = 0,1,2,...) \tag{A11}$$